

2

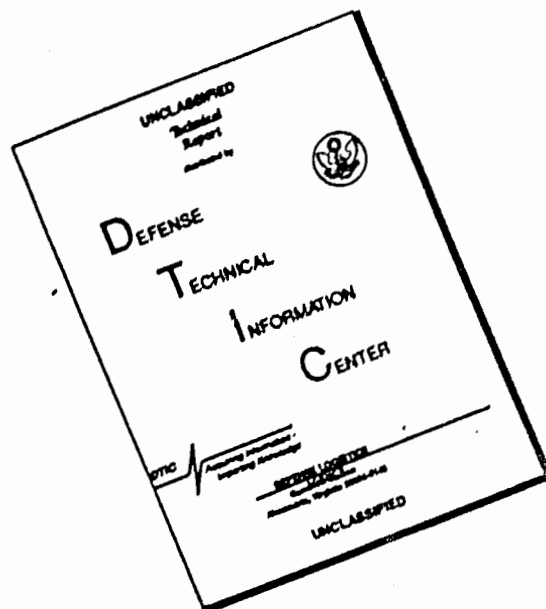
AD A 121 691

REPORT DOCUMENTATION PAGE		READ INSTRUCTIONS BEFORE COMPLETING FORM
1. REPORT NUMBER <b>AFOSR-TR- 82-1006</b>	2. GOVT ACCESSION NO. <b>AD-A121691</b>	3. RECIPIENT'S CATALOG NUMBER
4. TITLE (and Subtitle) <b>UNSTEADY TURBULENT BOUNDARY LAYERS IN ADVERSE PRESSURE GRADIENTS</b>		5. TYPE OF REPORT & PERIOD COVERED <b>INTERIM</b>
6. AUTHOR(s) <b>E E COVERT P F LORBER</b>		6. PERFORMING ORG. REPORT NUMBER <b>AFOSR-80-0282</b>
7. PERFORMING ORGANIZATION NAME AND ADDRESS <b>DEPARTMENT OF AERONAUTICS &amp; ASTRONAUTICS MASSACHUSETTES INSTITUTE OF TECHNOLOGY CAMBRIDGE, MA 02139</b>		10. PROGRAM ELEMENT, PROJECT, TASK AREA & WORK UNIT NUMBERS <b>61102F 2307/A2</b>
11. CONTROLLING OFFICE NAME AND ADDRESS <b>AIR FORCE OFFICE OF SCIENTIFIC RESEARCH/NA BOLLING AFB, DC 20332</b>		12. REPORT DATE <b>June 1982</b>
14. MONITORING AGENCY NAME & ADDRESS (if different from Controlling Office)		13. NUMBER OF PAGES <b>13</b>
		15. SECURITY CLASS. (of this report) <b>UNCLASSIFIED</b>
		15a. DECLASSIFICATION/DOWNGRADING SCHEDULE
16. DISTRIBUTION STATEMENT (of this Report) <b>Approved for Public Release; Distribution Unlimited.</b>		
17. DISTRIBUTION STATEMENT (of the abstract entered in Block 20, if different from Report)		
18. SUPPLEMENTARY NOTES <b>Proceedings of the AIAA/ASME Joint Thermophysics, Fluids, Plasma and Heat Transfer Conference 3rd, St Louis, MO, 7-11 June 1982, AIAA 1290 Avenue of the Americas, NY NY 10104 1982</b>		
19. KEY WORDS (Continue on reverse side if necessary and identify by block number) <b>UNSTEADY FLOW BOUNDARY LAYERS FLUID MECHANICS AIRFOIL AERODYNAMICS</b>		
20. ABSTRACT (Continue on reverse side if necessary and identify by block number) <b>A number of characteristics of an unsteady turbulent boundary layer have been measured on the after part of the upper surface of an 0012 airfoil (<math>X/c = .69</math> and <math>.94</math>). The data is taken at chord Reynolds number of 700,000 and over a range of reduced frequencies (based upon the semichord) of 0.5 to 6.4. Mean and unsteady velocity profiles, as well as Reynolds stress profiles, are presented, as is the nonlinear coupling from the unsteady motion into the steady motion. Data is presented and discussed which shows that for this experiment the periodic unsteady turbulent velocity profile tends toward a universal shape.</b>		

DTIC  
ELECTIC  
NOV 22 1982  
S E D

DTIC FILE COPY

# DISCLAIMER NOTICE



THIS DOCUMENT IS BEST QUALITY AVAILABLE. THE COPY FURNISHED TO DTIC CONTAINED A SIGNIFICANT NUMBER OF PAGES WHICH DO NOT REPRODUCE LEGIBLY.

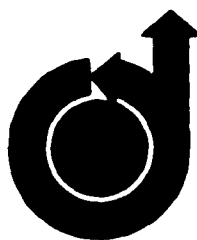
AFOSR-TR- 82 - 1006

**AIAA-82-0966**

**Unsteady Turbulent Boundary Layers in  
Adverse Pressure Gradients**

E.E. Covert and P.F. Lorber,  
Massachusetts Institute of Technology,  
Cambridge, MA

Accession For	
NTIS GRA&I	<input checked="" type="checkbox"/>
DTIC TAB	<input type="checkbox"/>
Unannounced	<input type="checkbox"/>
Justification	
By	
Distribution/	
Availability Codes	
Avail and/or	
Dist	Special
A	



**AIAA/ASME 3rd Joint Thermophysics,  
Fluids, Plasma and Heat Transfer  
Conference**

June 7-11, 1982/St. Louis, Missouri

For permission to copy or republish, contact the American Institute of Aeronautics and Astronautics,  
1290 Avenue of the Americas, New York, NY 10104. For public release,  
distribution unlimited.

82 11 22 014

UNSTEADY TURBULENT BOUNDARY LAYERS  
IN ADVERSE PRESSURE GRADIENTS

Eugene E. Covert\*

Peter F. Lorber\*\*

Department of Aeronautics and Astronautics  
Massachusetts Institute of Technology  
Cambridge, Massachusetts 02139

Abstract

A number of characteristics of an unsteady turbulent boundary layer have been measured on the after part of the upper surface of an O012 airfoil ( $\chi/c = .69$  and  $.94$ ). The data is taken at chord Reynolds number of 700,000 and over a range of reduced frequencies (based upon the semichord) of 0.5 to 6.4. Mean and unsteady velocity profiles, as well as Reynolds stress profiles, are presented, as is the non-linear coupling from the unsteady motion into the steady motion. Data is presented and discussed which shows that for this experiment the periodic unsteady turbulent velocity profile tends toward a universal shape, independent of the mean adverse velocity gradient, at higher reduced frequencies.

Nomenclature

a	elliptic cylinder minor axis
b	elliptic cylinder major axis
c	airfoil chord
$c_f$	skin friction coefficient $\tau_w/\frac{1}{2} \rho U_\infty^2$
$c_p$	pressure coefficient, $(P-P_\infty)/\frac{1}{2} \rho U_\infty^2$
H	boundary layer shape parameter, $\delta^*/\theta$
k	reduced frequency, $\omega c/2U_\infty$
p	pressure
$Re_\theta$	Reynolds number based on momentum thickness $U_e \theta/\nu$
$U_e$	external velocity
$U_\infty$	freestream velocity
U	velocity component parallel to surface
$U_\tau$	friction velocity, $\sqrt{\tau_w/\rho}$
V	velocity component normal to surface
x	coordinate parallel to surface
y	coordinate normal to surface
$\alpha$	airfoil angle of attack
$\beta$	pressure gradient, $\frac{\delta^*}{\tau_w} \frac{dp}{dx}$
$\Gamma$	pressure gradient, $\frac{\theta}{U_e} \frac{dU_e}{dx} (Re_\theta)^{1/4}$
$\delta^*$	displacement thickness, $\int_0^\infty (1-u/U_e) dy$
$\theta$	momentum thickness, $\int_0^\infty u/U_e (1-u/U_e) dy$
$\nu$	kinematic viscosity
$\rho$	density
$\tau_w$	shear stress at the surface

$\omega$	radian frequency
$\bar{\quad}$	time average
$\sim$	period component
$\langle \quad \rangle$	ensemble average, $\langle u \rangle = \bar{u} + \tilde{u}$
'	nonperiodic fluctuating component of zero mean, $u = \langle u \rangle + u'$

Introduction

Recently L. W. Carr<sup>1</sup> presented a survey of the state-of-the-art of measurements on unsteady turbulent boundary layers. In many of these experiments the metric surface is a flat plate of one wall of the wind tunnel. Unsteadiness is frequently introduced by oscillating vanes or shutters located either upstream or downstream of the test surface. Of all the experiments cited, those of Karlsson<sup>2</sup>, Patel<sup>3</sup>, Kenison<sup>4</sup>, Schachenmang and Rockwell<sup>5</sup>, Simpson, Shivaprasad and Chew<sup>6</sup>, and Cousteix, Houdeville and Raynaud<sup>7</sup> have produced data that are perhaps most closely related to that which will be presented below. Several years ago Telionis<sup>8</sup> reviewed the state of understanding of both separated and attached unsteady boundary layers. He concluded that,

- generally the mean profiles are affected very little by the unsteadiness,
- the pressure gradient has a strong effect on the fluctuations, and
- the state-of-the-art of turbulence modeling is inadequate.

An example of the latter is calculations that predict an overshoot in unsteady velocity amplitude of 1-2% over that at the edge of the boundary layer, while the data shows overshoots of 10 times that value for the same conditions. Telionis concluded something fundamental was missing from the models.

In this paper, we will present additional data that characterizes the unsteady turbulent boundary layer. Our metric surface is the upper surface of a N.A.C.A. 0012 airfoil which is fixed in a wind tunnel. As described below the unsteady flow is generated by aerodynamic interference at the trailing edge. We will present data on  $\langle u \rangle$ ,  $\langle v \rangle$ ,  $\langle v'^2 \rangle$  and  $\langle u'v' \rangle$  and offer some comments on the processes and their limits.

Location of Experiment

The experiment we are conducting is somewhat different in configuration from those referred to in the introduction. As indicated in the introduction, our metric surface is a N.A.C.A. 0012 airfoil, with chord length 50.8 cm. It is located between two vertical sidewalls in the MIT Wright Brothers' Wind Tunnel. The walls are not quite parallel to the flow, rather they diverge enough to compensate for the effects of

\*Fellow and Member AIAA, Professor of Aeronautics & Astronautics, MIT

\*\*Student Member, Research Assistant, Department of Aeronautics and Astronautics, MIT

boundary layer growth. Preliminary data taken by Kanevsky<sup>9</sup> on a flat plate with a 25 micro inch surface installed in place of the airfoil showed that the  $C_p$  on the plate was uniform to within  $\pm 1\%$  over the entire plate and  $\pm .3\%$  over the metric zone (Fig. 1). The measured velocity profiles were expressed in the form of the law of the wall as (Fig. 2)

$$\frac{u}{u_\tau} = 2.5 \ln \frac{yu_\tau}{\nu} + 5.5$$

The pressure distribution on the airfoil surface due to the unsteady flow generated by the rotating ellipse is described in detail in Ref. 10 and 11. For convenience some results of the pressure measurements are summarized here. The current boundary layer experiments were performed at a tunnel velocity of 20 mps, resulting in a Reynolds number based on airfoil chord of  $7 \times 10^5$ . At this velocity the freestream turbulence level is approximately 0.7%. Figures 4 and 5 show the mean pressure coefficient distributions for this Reynolds number, for reduced frequencies  $k = 0.5$  to 6.4, and for mean angle of attack of 0 and 10 degrees. Figures 6 and 7 illustrate the ensemble averaged fundamental harmonic pressure coefficient amplitude and phase lag distributions seen at 0 and 10° angle of attack for the upper surface of the airfoil. Upper surface mean and unsteady amplitudes increase smoothly near the trailing edge, while the phase lag in this region is nearly constant. Note both amplitude and phase distributions shown in Figs. 6 and 7 were relatively independent of the geometric angle of attack, as long as the airfoil has not stalled.

Following Clauser<sup>12</sup>, we could define the non-dimensional pressure gradient  $\frac{x}{\alpha} \frac{dp}{dx}$ , which for steady flow is equal to  $-\frac{2x}{U_e} \frac{dU_e}{dx}$ , a quantity independent of Reynolds number. The mean value of this parameter at the boundary layer measurement locations ranges for the present test from + 0.25 to + 1.7. Clauser gives 0.58 as the maximum pressure gradient for equilibrium profiles. Similarly, for the unsteady pressure distribution, the unsteady amplitude of  $\frac{x}{q} \frac{dp}{dx}$  ranged from .02 to .40. The experimental conditions are given in Tables 1 and 2.

Buri's form of the mean-nondimensional pressure gradient,  $\Gamma = \frac{\theta}{U_e} \frac{dU_e}{dx} (Re_\theta)^{1/4}$  is also useful in defining test conditions. For our profiles,  $\Gamma$  was between -.002 and -.042.  $\Gamma \sim -.06$  corresponds to separation, for a steady mean flow<sup>13</sup>.  $\Gamma$  may be written in steady flow as  $\frac{\rho}{40C_f} \frac{1}{U_c} \frac{dU_e}{dx}$  which is closely related to Clauser's alternate form  $B = \frac{\delta^*}{\tau_w} \frac{dp}{dx}$ . The advantage of Clauser's  $\beta$  or Buri's  $\Gamma$  is that the boundary layer history is implicitly included.\*

Boundary layer velocities were measured using either a single hot wire (determining longitudinal velocity) or a cross wire (determining both longitudinal and normal velocities). The velocity probes were motor driven across the boundary layer, with the position being given by a linear potentiometer. Flow corporation constant temperature anemometers, linearizers and sum difference amplifiers were used to produce  $u$  and  $v$  velocities.

With the exception of some of the low pressure gradient data, for which an analog system was used, the velocities and pressures were digitized, ensemble averaged, converted to nondimensional form and plotted on line (Fig. 8). This procedure allowed monitoring of the progress of the experiment, and in particular indicated when additional cycles of data were needed in order to properly define the unsteady quantities. The required number of cycles depends on the signal to noise ratio of the periodic to fluctuating amplitudes, and ranges from 100 to 4096.

For data taken with the single hot wire, only  $\langle u \rangle = u + \bar{u}$  and  $\langle u'u' \rangle$  were obtained, while data\*\* taken with the cross wire also included  $\langle v \rangle$ ,  $\langle u'v' \rangle$ ,  $\langle v'v' \rangle$ ,  $\langle u'v' \rangle$ , where  $u'$  is defined to have zero time average and ensemble average. This data will be stored on tape and provided to Dr. L.W. Carr at Ames Research Center<sup>1</sup>.

\*That is, Karman's integral relation may be used to relate  $\beta$  or  $\Gamma$  to the flow in the boundary layer.

$$\beta = \frac{\delta^*}{\tau_w} \frac{dp}{dx} = \frac{H}{H+2} \left\{ \frac{U_e^2}{U_\tau^2} \frac{d\theta}{dx} - 1 \right\}$$

$$\Gamma = \frac{\theta}{80\tau_w} \frac{dp}{dx} = \frac{-1}{80(H+2)} \left\{ \frac{U_e^2}{U_\tau^2} \frac{d\theta}{dx} - 1 \right\}$$

Hence either Clauser's  $\beta$  or Buri's  $\Gamma$  are measures of a departure of the turbulent boundary layer from the flat plate equilibrium flow. If  $\beta$  or  $\Gamma$  are pure constants (ie, independent of Reynolds number) then the flow in question is selfsimilar. In any case  $\beta$  or  $\Gamma$  represent the ratio of two forces; one is force per unit volume applied to the boundary layer from outside the boundary layer and the other is the force per unit volume applied by the wall through the shear stress; where the volume is normalized to either the displacement or momentum defect thickness. The presence of the products of boundary parameters implies the unsteady boundary layer offers the possibility for rectification and multiples of the fundamental frequency of excitation.

\*\*Note the decomposition

$$u = \bar{u} + \hat{u} + u'$$

only implies that  $u'$  has a zero temporal mean. There is no intent to imply that  $u'$  is independent of frequency of excitation, ie, in the notation of Ref. 14

$$u'(x,y,t) = u'_0(x,y,t) + u'_1(x,y,t)e^{i\omega t}$$

except that we normalize  $u'_1$  such that  $u'_1 \rightarrow 0$  as  $\omega \rightarrow 0$

TABLE I. SUMMARY OF EXPERIMENTAL CONDITIONS

k	$\alpha$	x/c	$\bar{\Gamma}$	$\bar{\theta}/c$	$\bar{H}$	$\overline{Re}_\theta$	$\frac{x}{q} \frac{dP}{dx}$	$\frac{x}{q} \frac{dP}{dx}$	$\frac{U_e}{U_e}$
0.5	$0^\circ (1)$	0.69	-0.0025	.0016	1.80	1160	.381	.0483	.021
1.0			-0.0019	.0016	1.71	1170	.281	.0593	.022
1.5			-0.0032	.0017	1.74	1340	.422	.0575	.014
2.0			-0.0023	.0016	1.75	1230	.334	.0299	.0057
3.9			-0.0024	.0018	1.74	1410	.297	.0198	.0034
6.4			-0.0021	.0019	1.74	1430	.255	.0375	.0038
0.5	$0^\circ (1)$	0.94	-0.0144	.0025	1.64	1570	1.71	.273	.031
1.0			-0.0151	.0026	1.71	1670	1.68	.402	.038
2.0			-0.0138	.0025	1.61	1670	1.62	.203	.013
6.4			-0.0101	.0025	1.61	1780	1.19	.224	.0078
0.5	$10^\circ (1)$	0.94	-0.0408	.0090	2.38	5950	.969	.173	.020
1.0			-0.0358	.0088	2.50	5600	.891	.228	.033
2.0			-0.0401	.0091	2.18	5980	.951	.088	.0076
3.9			-0.0406	.0093	2.04	6120	.947	.089	.0048
6.4			-0.0430	.0095	2.00	6390	.958	.109	.0062
0.5	$10^\circ (2)$	0.94	-0.0297	.0093	2.56	6390	.672	.238	.040
1.0			-0.0322	.0094	2.53	6230	.725	.262	.047
2.0			-0.0297	.0092	2.44	6160	.689	.153	.016
3.9			-0.0306	.0087	2.22	6420	.743	.135	.0088
6.4			-0.0304	.0083	2.11	6400	.769	.166	.0079

(1) Cylinder axis at x/c = 1.18, y/c = -.28

(2) Cylinder axis at x/c = 1.12, y/c = -.19

TABLE II. STEADY STATE TEST CONDITIONS

ELLIPSE ORIENTATION	$\alpha$	x/c	$\Gamma$	$\theta/c$	$Re_\theta$	H	$\frac{x}{q} \frac{dP}{dx}$
HORIZ.	$0^\circ (1)$	.69	-0.0017	.0013	970	1.81	.55
VERT.			-0.0032	.0020	1500	1.87	.57
HORIZ.	$0^\circ (1)$	.94	-0.011	.0022	1410	1.66	1.58
VERT.			-0.037	.0047	2900	1.90	1.67
HORIZ.	$10^\circ (2)$	.94	-0.034	.0075	4910	2.30	.80
VERT.			-0.0078	.0107	7380	3.40	.13

(1) cylinder axis at x/c = 1.18, y/c = -.28

(2) cylinder axis at x/c = 1.12, y/c = -.19

Section omitted from page 2 (after the first equation).

This is in general agreement with other flat plate turbulent boundary layer data. Thus we feel that the mean effects of the installation have been minimized.

The airfoil may be rotated about the trailing edge to give a mean geometric angle of attack of between 0 and 15 degrees. Just downstream of and below the the trailing edge, a two dimensional elliptic cylinder ( $b/a = 2.12$ ) is located, with its axis at either  $x/c = 1.175$ ,  $y/c = -.276$  or  $x/c = 1.12$ ,  $y/c = -.19$ . This elliptic cylinder is rotated at from 0 to 3000 r.p.m., through a belt driven by an adjustable speed electric motor. This provides an unsteady perturbation to the flow angle at the trailing edge. The apparatus and its installation is shown in figure 3.

## Experimental Results

The experimental results are presented in terms of mean profiles for the velocities and Reynolds stresses, and Fourier amplitudes and phase lags for these quantities. Only fundamental harmonic (twice the elliptic cylinder rotation rate) data is presented.

Figure 9 shows two cases of steady flow mean velocity profiles at  $x/c = .94$ ,  $\alpha = 0$ , corresponding to horizontal and vertical elliptic cylinder orientations. Figure 10 shows the identical quantities for  $\alpha = 10^\circ$ . The difference between the velocities at the horizontal and vertical orientations is the quasi-steady amplitude of the system. Note that the profiles with a steady vertical elliptic cylinder are closer to separation, and correspond to much thicker boundary layers.

The graph of mean  $u$  velocity versus distance is shown in Fig. 11 for the case where the elliptic cylinder was rotating at  $k = 0.5$ . Three curves are plotted, corresponding to three local mean pressure gradients,  $\Gamma = -.0025$ ,  $-.014$ ,  $-.041$ . The same geometric situation is replotted in Fig. 12 for  $k = 6.4$ . The increasing pressure gradient makes the profile fuller near the wall and more concave near the outer edge of the boundary layer.

The mean velocity profiles at approximately the same local mean pressure gradient of  $\Gamma \approx -.014$ , for 4 reduced frequencies  $k = 0.5, 1.0, 2.0$  and  $6.4$  are shown in Fig. 13. Except for the  $k = 6.4$  case for which  $\Gamma$  is slightly smaller, the differences between the profiles are no greater than the experimental error. This slight difference in Buri's pressure gradient parameter is probably due to the increased mean circulation resulting from higher cylinder rotation rate. The effect of  $k$  on the mean pressure distribution when  $\alpha = 0$  was shown in Fig. 4.

However, for the higher pressure gradient case,  $\Gamma = -.030$ , seen in Fig. 14, differences due to reduced frequency are clear. Increasing reduced frequency has a similar effect on the profiles as reduced pressure gradient. The inflection of the profiles is reduced, thus the profile looks less like a separation profile.

Ensemble averaged velocity profiles are plotted in Fig. 15 for mean pressure gradient  $\Gamma = -.014$  and reduced frequency 0.5. The profiles give the ensemble averaged velocity versus distance for several representative times in the rotational cycle. For this pressure gradient all profiles are without inflection points at all times. The reduced unsteady amplitudes at high frequencies are seen in Fig. 16, for  $\Gamma = -.010$  and  $k = 6.4$ . All profiles remain well behaved.

Fig. 17, for  $k = 0.5$  and  $\Gamma = -.041$  shows quite different character, as the profile shifts from large inflection and incipient separation to no inflection during the rotation cycle. Figure 18 illustrates higher frequency  $k = 6.4$  at  $\Gamma = -.043$ . Note a moderately inflected profile is maintained throughout the cycle probably due to smaller unsteady amplitudes. These differences with time for the low frequency case are quite similar to those exhibited by the steady profiles (Figs. 9 and 10).

The unsteady velocity data of last four figures may also be reduced to distributions of Fourier amplitude and phase lag across the boundary layer. Figure 19 presents the amplitude of the fundamental harmonic, normalized by the amplitude of the same harmonic of the external flow, for the same cases as Fig. 13,  $\Gamma \approx -.014$ ,  $k = 0.5, 2.0, 6.4$ . The high scatter seen for  $k = 6.4$  is a result of an insufficient number of averages for the relatively small velocity amplitude present. The most striking feature of these plots is the large value of the unsteady amplitude overshoot, which ranges from 2.4 at  $k = 0.5$  to 1.7 at  $k = 6.4$ . As will be discussed below, these values are quite similar to previous results for similar mean profiles. The height at which this maximum occurs also decreases with increasing reduced frequency.

Figure 20 shows the same quantities at a higher pressure gradient,  $\Gamma = -.030$ . In addition, the vertical velocity amplitude  $\hat{v}$  is also shown. As in the lower  $\Gamma$  case, the maximum  $u$  amplitude overshoot occurs at  $k = 0.5$  with lower values for  $k = 1.0, 2.0$  and  $6.4$ . However the height of this maximum decreases less rapidly with increasing reduced frequency than in the data shown in Fig. 19. The  $\hat{v}$  amplitudes all drop smoothly to 0 at the wall.

Comparing Figs. 19 and 20, the effect of pressure gradient is much more apparent for lower frequencies, as the maximum overshoot increases from 2.4 times the external amplitude to 5.6 times the external amplitude at  $k = .5$ , while remaining nearly constant for  $k = 6.4$ . The height of the maximum, at constant  $k$ , also increases for higher pressure gradients.

The next property of the velocity profiles to be illustrated are the mean nondimensional Reynolds stresses. Figure 21 shows  $\overline{u'u'}$  for the steady conditions of Fig. 9. Note the large difference in profile shape between the high and low pressure gradient states. Increased pressure gradient increases and broadens the maximum  $\overline{u'u'}$ , removing the sharp peak near the wall. The time average value of  $\overline{u'u'}$  in the presence of the unsteady flow is shown in Fig. 22 for  $\Gamma = -.014$  and  $\Gamma = -.010$ . Because this data was recorded in analog form, the experimental scatter was larger than for data recorded digitally, such as in Fig. 24. Nevertheless, these profiles do show the peak very close to the surface, such as was observed for Patel's zero pressure gradient results<sup>3</sup>, and in the low  $\Gamma$  steady data of Fig. 21. Values of  $\overline{u'u'}$  to compare with the higher pressure gradient steady case of Fig. 10 are shown in Fig. 23. The position of the maximum has moved further from the wall, and the maximum has increased to .025 for the nearly separated case. Data taken with the cross wire and the digital data acquisition system, which include measurement of all three quantities,  $u'u'$ ,  $v'v'$ , and  $u'v'$ , are shown in Fig. 24. For this higher pressure gradient ( $\Gamma = -.030$ ) case, both  $u'u'$  and  $v'v'$  appear independent of  $k$ , while  $u'v'$  is smaller for  $k = 0.5$  than for higher frequencies. The major effect of the increased pressure gradient is to remove the near wall peak in  $u'u'$ , and to increase the maximum value by a factor of three, from .0052 to .015. This effect is similar to the effect of the pressure gradient on the unsteady amplitude discussed above.

Finally, the amplitude of the fundamental harmonic of  $\langle u'u' \rangle$  for  $\Gamma = -.030$  and  $k = 0.5, 2.0$  and  $6.4$  is shown in Fig. 25. Two peaks are seen, the largest somewhat above the position of maximum mean Reynolds stress  $\overline{u'u'}$ , and the second close to the wall. All amplitudes decrease sharply as frequency is increased, for example, the maximum of  $\langle u'u' \rangle$  is .0085 at  $k = .5$ , but only .0003 at  $k = 6.4$ . This is probably due to both the decreased external  $\langle u \rangle$  amplitude and the decreased maximum ratio of  $\langle u \rangle$  to the external value. Figure 26 shows amplitudes for the three quantities  $\langle u'u' \rangle$ ,  $\langle u'v' \rangle$ , and  $\langle v'v' \rangle$  for the case  $k = 0.5$ ,  $\Gamma = -.030$ . The characteristic double maximum is seen in each curve, however, the height of the upper maximum differs.

#### Discussion

As mentioned previously, for high reduced frequencies,  $k > 2.0$ , the unsteady  $u$  profile tends to become independent of pressure gradient, and only weakly dependent on frequency. Figure 27 shows the ratio of the maximum unsteady amplitude to the external amplitude for all of the boundary layers presently studied, with  $-.002 < \Gamma < -.043$ . While large differences exist for  $k \leq 2$ , the higher  $k$  values definitely approach a common value of approximately 1.8.

Figure 27 also shows results from previous high frequency data. In computing a reduced frequency for flat plate experiments, a length equal to  $l/2$  the distance from the leading edge or from the boundary layer trip is used. These data, although generally of somewhat lower reduced frequency, do support the relative independence of the unsteady profile on pressure gradient and frequency. This result parallels theoretical predictions of Lighthill and Lin for laminar boundary layers<sup>15,16</sup>.

While not presented here in detail, phase distributions of  $\tilde{u}$  across the boundary layer were generally small and in agreement with those of Cousteix<sup>7</sup>. That is over the outer part of the boundary layer phase lags with respect to the outer flow of 10 to 20 degrees were observed, with the position of maximum lag corresponding to that of maximum amplitude. As the airfoil surface was approached the phase changed to a small lead (5-10°) over the external flow. Due to the relative sizes of the present hot wire probe and boundary layer, data in the viscous sublayer was not obtained.

The ensemble averaged profiles were normally the only data recorded. However, for selected data points, 15-25 cycles of raw data were stored. One result of the analysis of this data was an estimate of the magnitude of the coupling terms  $u'\tilde{u}$ ,  $v'\tilde{u}$ ,  $u'\tilde{v}$ ,  $v'\tilde{v}$ . These terms are commonly neglected<sup>3</sup>. Based on the present data the coupling terms were found to be at least one order of magnitude less than the equivalent turbulent terms,  $u'u'$ ,  $u'v'$ ,  $v'v'$ . It is likely that if more cycles were analyzed for this purpose the ratio would decrease even further. From a theoretical viewpoint such coupling terms should vanish if the ensemble average is taken at the same point in each cycle.

The unsteady portion of the ensemble averaged Reynolds stresses as shown in Fig. 25 as a Fourier amplitude is a different way of illustrating the phenomena observed previously in Reference 7. Cousteix, et al, show a time dependent variation in the maximum  $\langle u'v' \rangle$ . It varies from -.0055 to -.002, well within the range of the present data, i.e.  $\langle u'v' \rangle \sim -.00375 + .00175 \cos \omega t$  from the Fourier analysis cited above.

Figure 28 presents another significant feature of the ensemble averaged Reynolds stress: the phase lag across the boundary layer for a typical low frequency, high pressure gradient (and therefore high amplitude) case. The phase of  $\langle u'u' \rangle$  is seen to be about 180° different from that of  $\langle u \rangle$  over the outer boundary layer, with a shift taking place at approximately one mean momentum thickness from the wall, to becoming within 10° of being in phase with  $\langle u \rangle$ . In terms of the mean profile,  $\langle u \rangle$  and  $\langle u'u' \rangle$  are out of phase when  $\frac{d\bar{u}}{dy}$  and  $\frac{d}{dy}(\overline{u'u'})$  are of opposite sign, and in phase when they are of the same sign.

#### CONCLUSIONS

A series of experiments have been performed to determine the characteristics of the turbulent boundary layer of a NACA 0012 two dimensional airfoil subject to an oscillating external flow. Ensemble averaged velocities and Reynolds stresses were measured over a wide range of mean pressure gradients and reduced frequencies, from nearly quasi steady to significantly greater than a reduced frequency of unity, and from a mildly adverse gradient to one producing incipient separation.

Mean profiles were found to be quite independent of reduced frequency for moderate adverse pressure gradients, but for steeper adverse pressure gradients, the mean profile was less like a separation profile as the frequency was increased.

Periodic velocity profiles had large increases in amplitude in the boundary layer as compared to external flow, but small phase differences from that flow. For low frequencies, the profiles were highly dependent on the mean pressure gradient, while the high frequency profiles appeared to approach a universal profile independent of both frequency and pressure gradient.

Ensemble averaged Reynolds stresses had a much stronger dependence on the mean pressure gradient than on reduced frequency, with both high and low pressure gradient data being similar to previous results for roughly similar conditions.

Correlations between the periodic and non-periodic velocity components ( $u'\tilde{u}$ ) were found to be at least an order of magnitude smaller than the mean nonperiodic values ( $\overline{u'u'}$ ). Theoretically this value should be zero. The common neglect of these quantities appears to be justified.

A Fourier component of the ensemble averaged Reynolds stress was extracted from the data and was found to depend on the amplitude of the periodic velocities, and on the relative sign between the normal gradients of the mean velocity and mean Reynolds stress.

Acknowledgement

This project was sponsored under Grant <sup>AFO 52</sup> 80-0282 with USAF OSR, Dr. Michael S. Francis, Project Manager.

References

1. Carr, L.W., "A Compilation of Unsteady Turbulent Boundary Layer Experimental Data", AGARD AG-265, Nov. 1981.
2. Karlsson, S.F.K., "An Unsteady Turbulent Boundary Layer", *Journal of Fluid Mechanics*, 5 pg. 622, 1959.
3. Batel, M.H., "On Turbulent Boundary Layers In Oscillatory Flows", *Proc. Royal Soc. London A.*, 353 pp 121-144, 1977.
4. Kenison, R.C. "An Experimental Study of the Effect of Oscillating Flow on The Separation Region In A Turbulent Boundary Layer," AGARD-CP-227 Paper #20, Feb. 1978.
5. Schachenmann, A.A. and Rockwell, D.O., "Oscillating Turbulent Flow In A Conical Diffuser," *J. Fluids Engineering*, Dec. 1976, pp 695-701.
6. Simpson, R.L., Shivaprasad, B.G. and Chew, Y.T., "Some Important Features of Unsteady Separating Turbulent Boundary Layers", Presented at the IUTAM Symposium on Unsteady Turbulent Shear Flows, Toulouse, France, May 5-8, 1981
7. Couteix, J., Houdeville, R., and Raynaud, M., "Oscillating Turbulent Boundary Layer with Strong Mean Pressure Gradient", Presented at 2nd Symposium of Turbulent Shear Flows, Imperial College, London, 1979. (Also ONERA TP 1979-80).
8. Telionis, D.P., "Review Unsteady Boundary Layers, Separated and Attached", *J. Fluids Engineering*, 101, page 29, March 1979.
9. Kanevsky, A.R., "Comparison of Pressure Distribution for Circulation Generated by Angle of Attack with that Generated by Trailing Edge Perturbation," S.M. Thesis, M.I.T. Feb. 1978.
10. Lorber, P.F. and Covert, E.E., "Unsteady Airfoil Pressures Produced by Periodic Aerodynamic Interference", *J. AIAA* Sept. or Oct. 1982.
11. Lorber, P.F., "Unsteady Airfoil Pressure Produced by Perturbation of the Trailing Edge Flow." SM Thesis, M.I.T., Feb. 1981
12. Clauser, F.H., "Turbulent Boundary Layers in Adverse Pressure Gradients", *J. Aeronautical Sciences*, Feb. 1954, pp 91-108.
13. Schlichting, H., "Boundary Layer Theory", Vol. 6, McGraw-Hill Book Co., New York, 1968, pg. 629.
14. Romaniuk, M.S. and Telionis, D.P., "Turbulence Models for Oscillating Boundary Layers", AIAA paper 79-0069.
15. Lighthill, M.J., "The Response of Laminar Skin Friction and Heat Transfer to Fluctuations in the Stream Velocity," *Proc. Royal Soc. A.*, 229 1-23, 1954.
16. Lin, C.C., "Motion in the Boundary Layer with a Rapidly Oscillating External Flow," *Proc. 9th Int. Congr. App. Mech.*, Brussels, Vol. 4, pp 155-167, 1956.

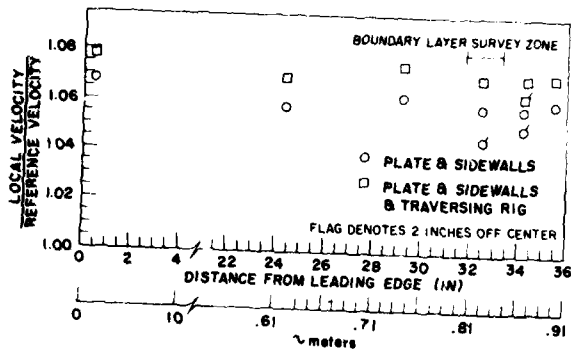


Fig. 1 External Velocity Distribution on Flat Plate

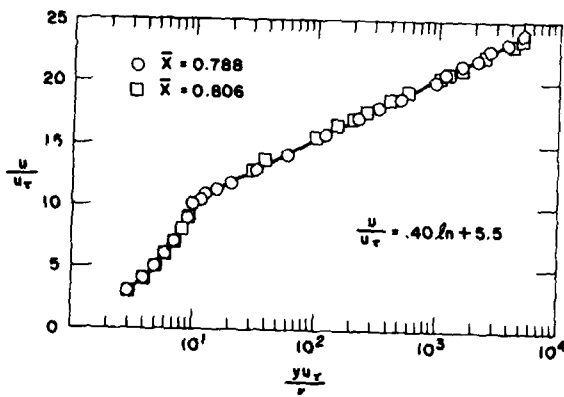


Fig. 2 Mean Velocity Profile on Flat Plate

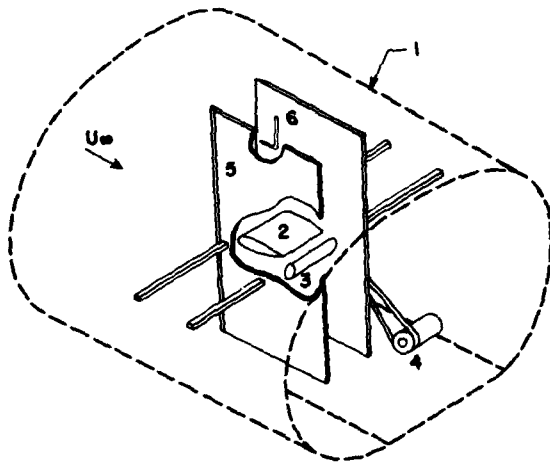


Fig. 3 Schematic Diagram for Unsteady Airfoil Test

- 1) Test Section, 2) Airfoil,
- 3) Rotating Elliptic Cylinder,
- 4) Drive Motor, 5) Sidewalls,
- 6) Pitot-Static Probe

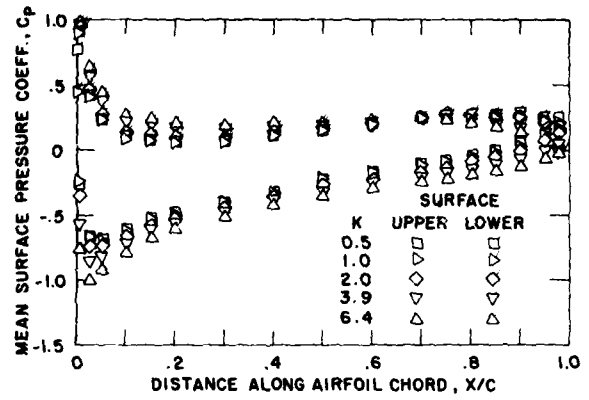


Fig. 4 Mean Airfoil Pressure Distributions,  $\alpha = 0^\circ$

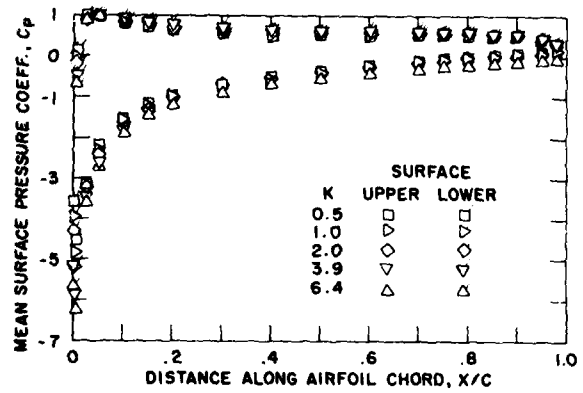


Fig. 5 Mean Airfoil Pressure Distributions,  $\alpha = 10^\circ$

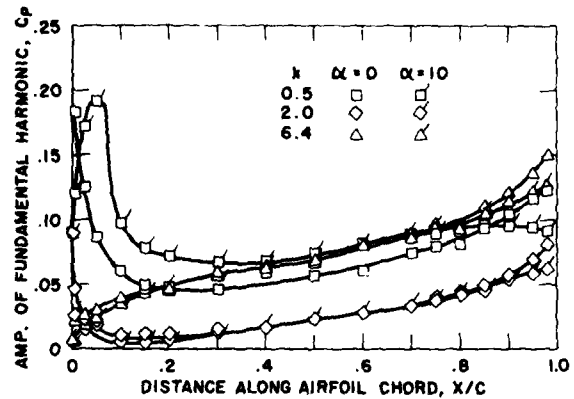


Fig. 6 Fundamental Harmonic Pressure Amplitude Distributions

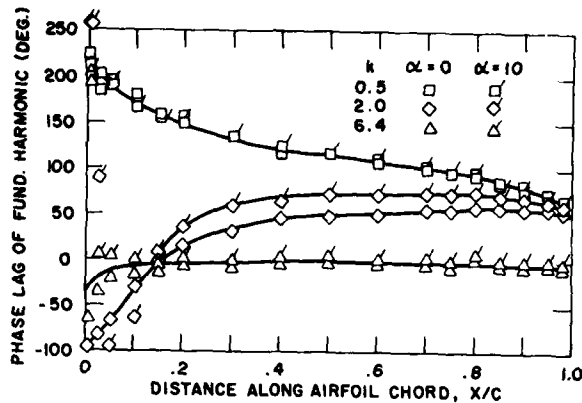


Fig. 7 Fundamental Harmonic Pressure Phase Lag Distributions

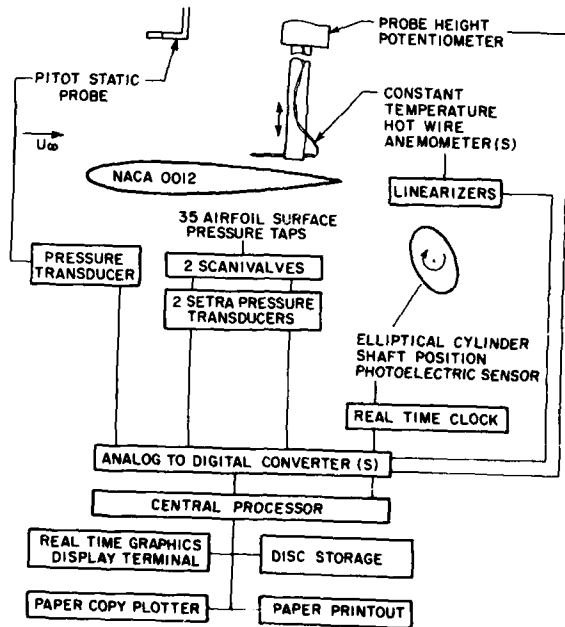


Fig. 8 Instrumentation Block Diagram

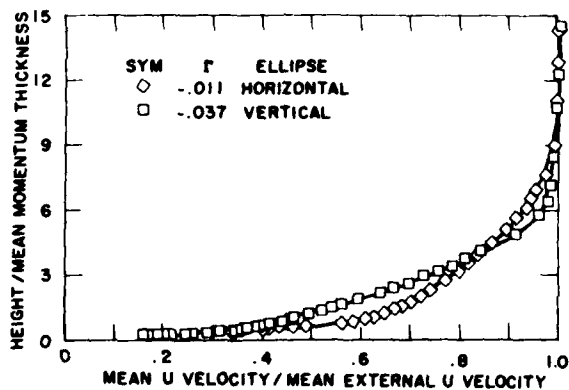


Fig. 9 Mean Velocity Profiles for Steady Elliptical Cylinder,  $\alpha = 0^\circ$

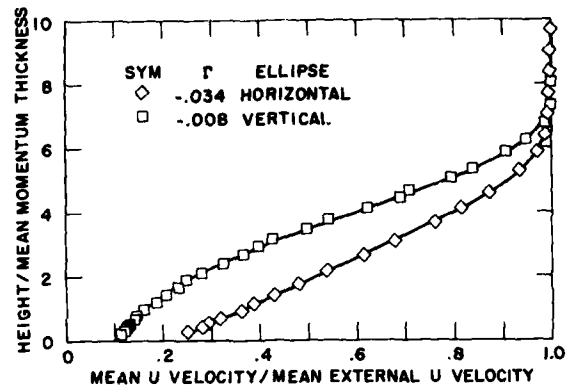


Fig. 10 Mean Velocity Profiles for Steady Elliptical Cylinder,  $\alpha = 10^\circ$

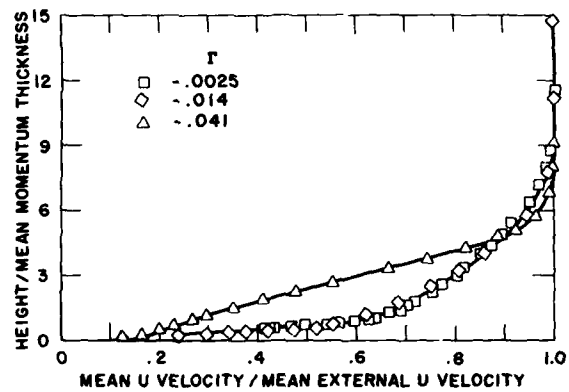


Fig. 11 Variation in Mean Velocity Profiles Due to Mean Pressure Gradient at Constant Reduced Frequency,  $k = 0.5$

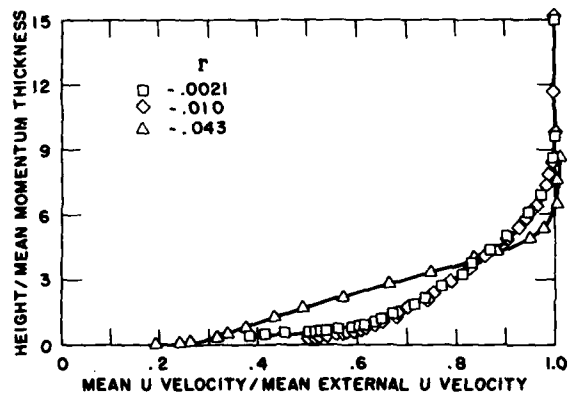


Fig. 12 Variation in Mean Velocity Profiles Due to Mean Pressure Gradient at Constant Reduced Frequency  $k = 6.4$

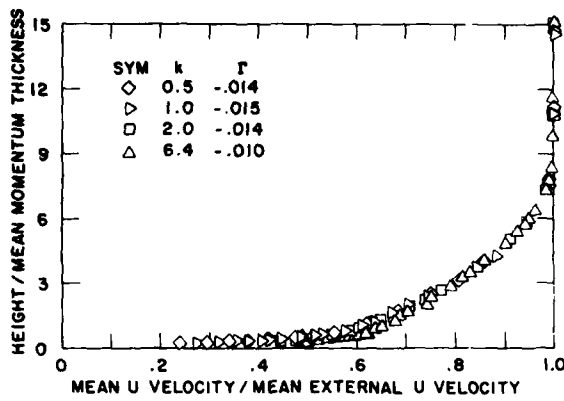


Fig. 13 Variation in Mean Velocity Profiles Due to Reduced Frequency at Constant Mean Pressure Gradient,  $\Gamma = -.014$

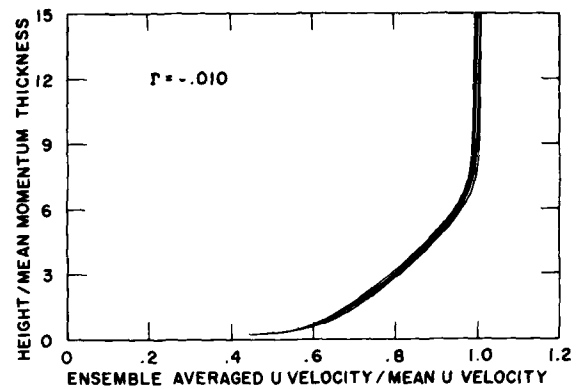


Fig. 16 Ensemble Averaged Velocity Profiles,  $k = 6.4, \Gamma = -.010$

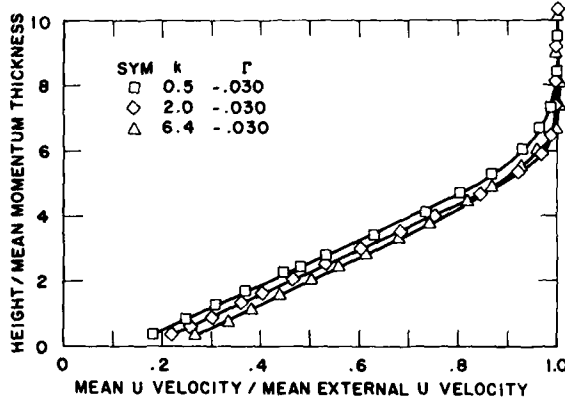


Fig. 14 Variation in Mean Velocity Profiles Due to Reduced Frequency at Constant Mean Pressure Gradient,  $\Gamma = -.030$

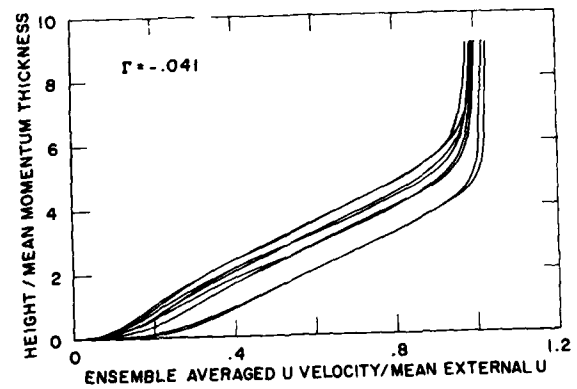


Fig. 17 Ensemble Averaged Velocity Profiles  $k = 0.5, \Gamma = -.041$

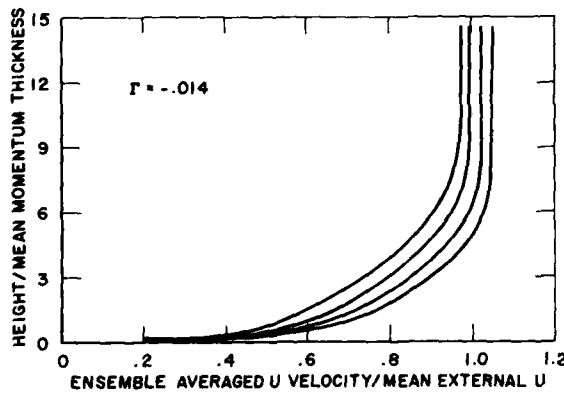


Fig. 15 Ensemble Averaged Velocity Profiles,  $k = 0.5, \Gamma = -.014$

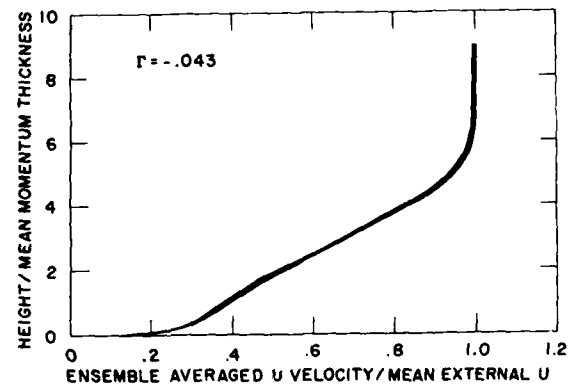


Fig. 18 Ensemble Averaged Velocity Profiles,  $k = 6.4, \Gamma = -.043$

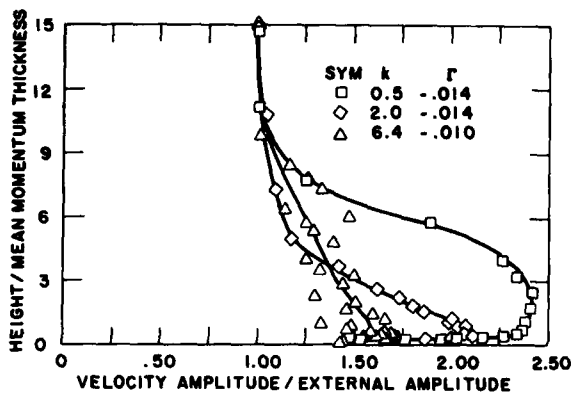


Fig. 19 Amplitude of Fundamental Harmonic  $u$  Velocity; Variation Due to Reduced Frequency at Fixed Mean Pressure Gradient,  $\Gamma = -.014$

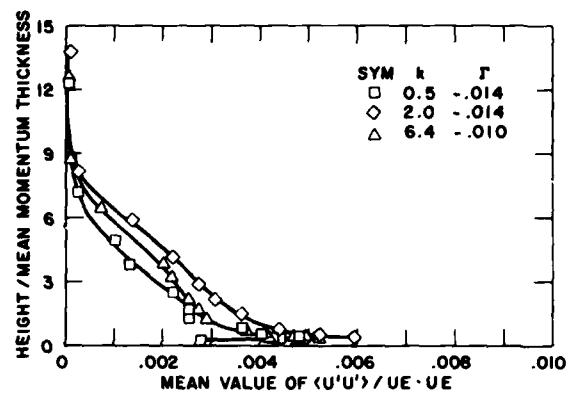


Fig. 22 Mean Reynolds Stress,  $\overline{u'u'}$ . Rotating Elliptic Cylinder and  $\alpha = 0^\circ$

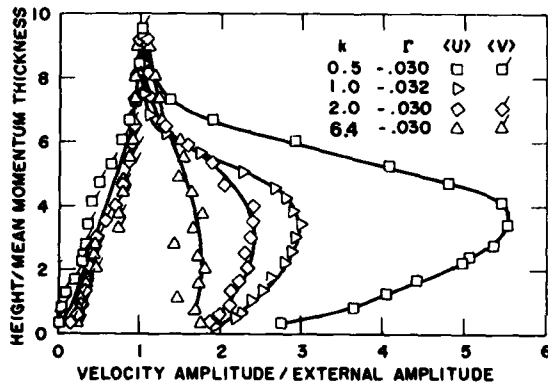


Fig. 20 Amplitude of Fundamental Harmonic  $u$  and  $v$  Velocity; Variation Due to Reduced Frequency at Fixed Mean Pressure Gradient,  $\Gamma = -.30$

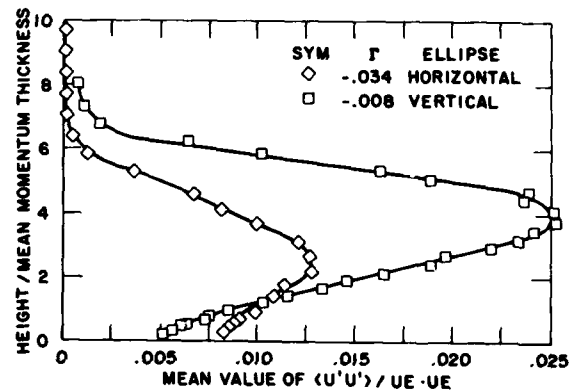


Fig. 23 Mean Reynolds Stress,  $\overline{u'u'}$ . Steady Elliptic Cylinder and  $\alpha = 10^\circ$

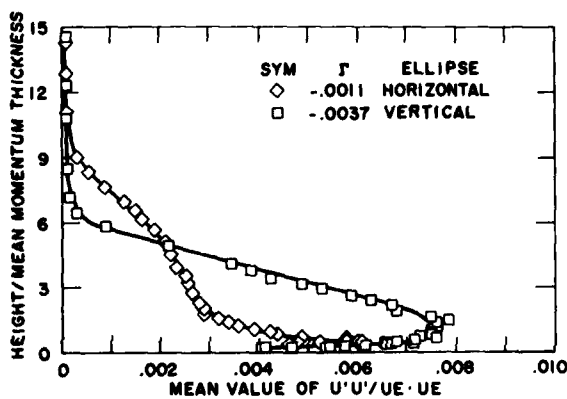


Fig. 21 Mean Reynolds Stress,  $\overline{u'u'}$ . Steady Elliptic Cylinder and  $\alpha = 0^\circ$

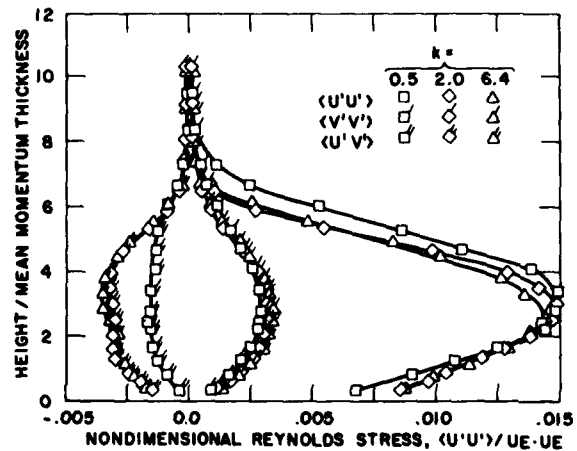


Fig. 24 Mean Reynolds Stresses,  $\overline{u'u'}$ ,  $\overline{v'v'}$  and  $\overline{u'v'}$ . Rotating Elliptic Cylinder and  $\alpha = 10^\circ$

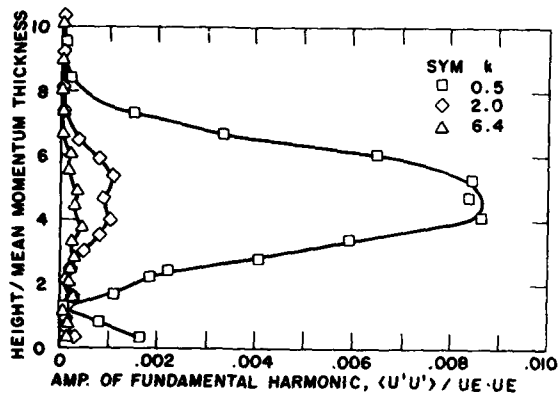


Fig. 25 Amplitude for the Fundamental Harmonic of the Ensemble Averaged Reynolds Stress,  $\langle u'u' \rangle$ . Variation with Reduced Frequency at  $\Gamma = -.030$

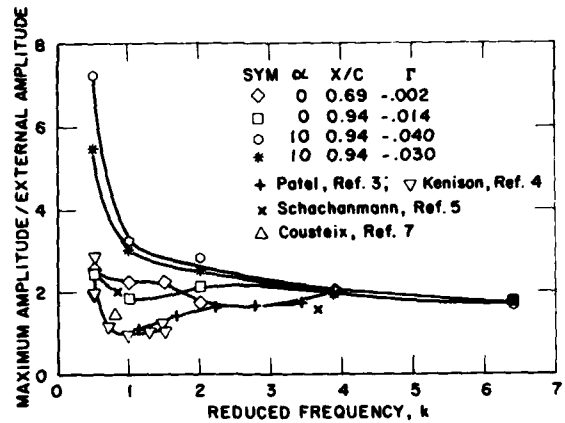


Fig. 27 Maximum Overshoot of the Fundamental Harmonic of the  $\langle u \rangle$  Velocity Plotted Against Reduced Frequency. Present and Previous Data are Compared

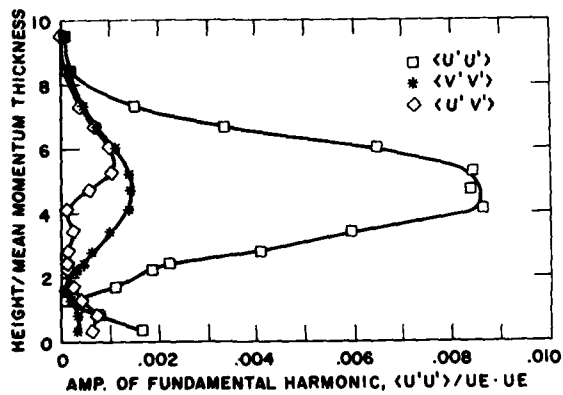


Fig. 26 Amplitude for the Fundamental Harmonic of the Ensemble Averaged Reynolds Stresses,  $\langle u'u' \rangle$ ,  $\langle v'v' \rangle$ ,  $\langle u'v' \rangle$ .  $k = 0.5$ ,  $\Gamma = -.030$

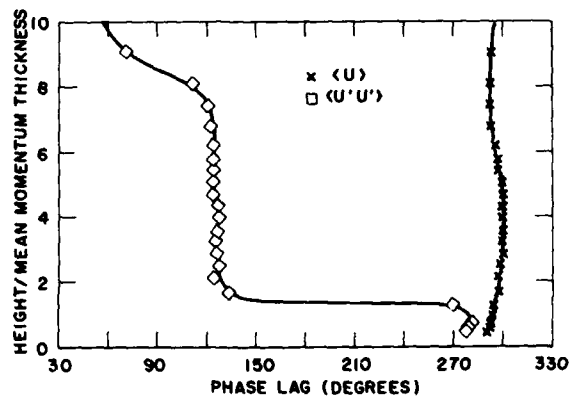


Fig. 28 Phase Lags for the Fundamental Harmonic of  $\langle u \rangle$  and  $\langle u'u' \rangle$ .  $k = 0.5$  and  $\Gamma = -.030$